Optical Engineering

SPIEDigitalLibrary.org/oe

Numerical analysis of the thermal and mechanical effects of laser windows of a high-power all-solid-state 2-μm laser system

Wenwen Liu
Yanxiong Niu
Haixia Liu
Caili Wang
Shuling Hu
Chao Zhang
Haisha Niu
Jiyang Li

SPIE

Numerical analysis of the thermal and mechanical effects of laser windows of a high-power all-solid-state 2-μm laser system

Wenwen Liu, Yanxiong Niu,* Haixia Liu, Caili Wang, Shuling Hu, Chao Zhang, Haisha Niu, and Jiyang Li
Beihang University, School of Instrument Science and Optoelectronic Engineering, No. 37 XueYuan Road, Haidian District, Beijing 100191, China

Abstract. The output window of a high-power laser system is vulnerable to damage, and this is the main limiting factor on the power scaling and structure integrity of the laser system. In endeavoring to obtain higher output powers from the laser system, the impact of the thermal and mechanical effects and the damage mechanism of the output window must be considered. In order to study these issues, a thermal model of the laser window is established based on the heat transfer and thermoelastic theories, and the expressions for the transient thermal and mechanical stress distributions of the output window are deduced in terms of the integral-transform method. Taking the infrared quartz window material as an example, the temperature and mechanical field distributions of a high-power all-solid-state 2-μm laser system window are simulated, and the laser-induced damage mechanism is deeply analyzed. The calculation results show that the laser window-induced damage is mainly caused by melting damage when the temperature exceeds the melting point of the material. The presented theoretical analysis and numerical simulation results are significant for the design and optimization of high-power laser windows. [DOI: 10.1117/1.OE.53.2.026102]

Keywords: laser window; temperature field; mechanical stress field; laser-induced damage mechanism.

Paper 131586 received Oct. 17, 2013; revised manuscript received Jan. 2, 2014; accepted for publication Jan. 6, 2014; published online Feb. 4, 2014.

1 Introduction

High-power all-solid-state 2-μm laser systems have played an increasingly important role in the technological landscape during the past few years. Applications have ranged from an abundance of medical uses, such as laser surgery and therapy, to more technical applications, such as laser ranging and remote sensing.[1–4] It is important to develop a laser system with high efficiency, long lifetime, and high stability; however, the laser output window may compromise the system's performance because of the thermal and mechanical effects caused by the window absorption in the process of high-power laser-beam outputting, which not only limits the service life, but also affects the power scaling of the system.[5] The thermal-mechanical effects and the damage mechanism of the laser output window have to be studied for further improving the power levels of the system before the onset of window damage.[6] These issues have received a great deal of attention, and various models have been proposed including the heating conduction model, the multiphoton ionization model, and cumulative ionization breakdown. Studies have shown[7,8] that the multiphoton ionization model and cumulative ionization breakdown dominate only in the case of high-power pulsed output, such situations have difficulties in quantitative analysis, and the heating conduction model is frequently used in the interpretation of continuous wave (cw) laser damage of output windows.[9]

In this article, we establish a three-dimensional (3-D) thermal model of the laser output window. Expressions for the transient thermal and mechanical distributions are deduced in the case of continuous laser output using the integral-transform method. Then, taking the infrared quartz window material as an example, the temperature and mechanical field distributions of a high-power all-solid-state 2-μm laser system window are simulated. Finally, the laser-induced damage mechanism is analyzed.

*Address all correspondence to: Yanxiong Niu, E-Mail: niuyx@buaa.edu.cn

2 Model Building

2.1 *2-μm Laser System*

The 2-μm Tm:YAG laser system contains a two-rod scheme, in which either rod employs a laser diode (LD) side-pumping laser module. The module contains five diode arrays, and each array consists of 12 diodes operating in cw-mode with a central wavelength of 785 nm. The rod is 4 mm in diameter and 69 mm in length with a Tm^{3+}-ion doping concentration of 3.5%. The Tm:YAG rod is cooled to 8°C by deionized water. M1 is the flat rear mirror coated to obtain a reflectivity more than 99.5% at 2 μm, and M2 is the output coupler with a transmission of 5% around 2 μm; in this instance, the wavelength of the output laser is 2.07 μm, and the maximum cw output power is 115 W. The schematic of the laser system is shown in Fig. 1 (Ref. 10).

The selection of the laser window is extremely important during the design of lasers. Materials such as CaF_2, Al_2O_3, and BaF_2 are commonly used for optical windows,[11] and quartz glass, specifically, exhibits outstanding thermodynamic properties, which makes it an attractive selection as the window material of a high-power 2-μm laser system.

2.2 *Thermal Model Description*

Heat deposition arises due to the absorption of the laser-beam energy when a high-energy laser beam passes through

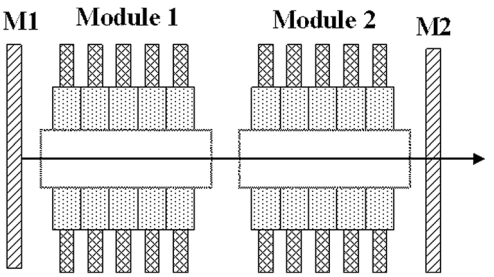

Fig. 1 Schematic of the laser system.

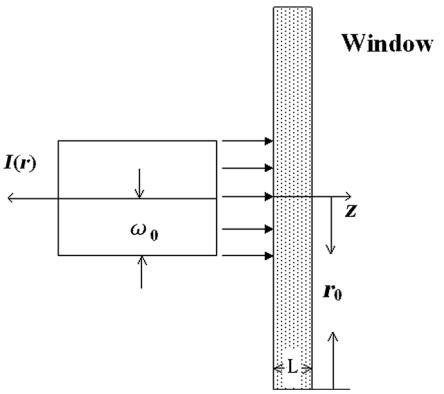

Fig. 2 Schematic of the thermal model of the output window.

the output window, resulting in temperature rise as well as thermal stress. The thermal model of the output window is defined and illustrated in Fig. 2. A laser beam with a radius ω_0 is incident along the positive z-direction for the window M2, which has a radius r_0 and a thickness L.

The 3-D heat transfer equation of the window can be expressed as

$$\frac{\partial^2 T}{\partial r^2}+\frac{1}{r}\frac{\partial T}{\partial r}+\frac{\partial^2 T}{\partial z^2}+\frac{q(r,z,t)}{k}=\frac{\rho C}{k}\frac{\partial T}{\partial t}, \tag{1}$$

where ρ, C, and k indicate the density, heat capacity, and thermal conductivity of the window material, respectively. High-power laser systems generally operate in a multimode state, and thus the laser beam can be assumed to be uniformly distributed. The heat source q, therefore, can be described as follows:

$$q(r,z,t)=\begin{cases} I_0 e^{-\alpha z} & 0\le r\le \omega_0, \quad t\ge 0 \\ 0 & \text{else} \end{cases}, \tag{2}$$

where α is the absorption coefficient of the material. I_0 is the peak power density, which can be described as

$$I_0=\frac{P_0(1-\tau)}{\pi\omega_0^2}, \tag{3}$$

where τ is the transmittance of the window, and P_0 represents the total beam power. The initial and boundary conditions are

$$\begin{cases} T=T_\infty & t=0 \\ \frac{\partial T}{\partial r}=0 & r=r_0 \\ \frac{\partial T}{\partial z}=0 & z=0,l \end{cases} \tag{4}$$

where T_∞ is the ambient temperature.

3 Theoretical Analysis

There are many analytical methods for solving Eq. (1) based on the initial and boundary conditions in Eq. (4).[12] Numerical methods, including the finite-element method[13,14] and the finite-difference method,[15] do not involve derivation of formulas or transformations, and so the solution procedure is convenient, especially in simulating multidimensional systems.[16] However, numerical solutions cannot provide an intuitive understanding of the relationships among the various physical data, whereas analytical solutions can clearly depict how the temperature-stress field distribution evolves with the parameters of the laser and window material.[17,18] Therefore, we employ the approach of using the integral-transform method to obtain such analytical solutions in this article.

Based on the model established above, we obtain the following formulas through utilizing the integral-transform method to solve Eqs. (1)–(4) and performing the positive and inverse integral transforms for variables r and z:[19]

$$T(r,z,t)=\sum_{m=1}^{\infty}\frac{R_0(\beta_m,r)}{N(\beta_m)}\bar{T}(\beta_m,z,t) \tag{5}$$

$$\bar{T}(\beta_m,z,t)=\int_{r\prime=0}^{r_0} r' R_0(\beta_m,r')T(r',z,t)\mathrm{d}r. \tag{6}$$

Here, $T(r,z,t)$ is the temperature distribution of the window, and Eq. (6) is the inverse transform of Eq. (5). The eigenfunctions $R_0(\beta_m,r)$ and the norm $N(\beta_m)$ are obtained as

$$R_0(\beta_m,r)=\begin{cases} J_0(\beta_m r) & m\ne 0 \\ 1 & m=0 \end{cases} \tag{7}$$

$$\frac{1}{N(\beta_m)}=\begin{cases} \frac{2}{r_0^2 J_0^2(\beta_m r_0)} & m\ne 0 \\ \frac{2}{r_0^2} & m=0 \end{cases}, \tag{8}$$

where the eigenvalues β_m are the positive roots of $J_1(\beta_m r_0)=0$, J_x refers to the x'th Bessel function, r is the radial coordinate, and r_0 is the window radius.

The eigenfunctions $Z(\eta_p,z)$ and the norm $N(\eta_p)$ are obtained as

$$Z(\eta_p,z)=\begin{cases} \cos\eta_p z & p\ne 0 \\ 1 & p=0 \end{cases} \tag{9}$$

$$N(\eta_p)=\begin{cases} \frac{2}{l} & p\ne 0 \\ \frac{2}{l} & p=0 \end{cases}, \tag{10}$$

where the eigenvalues η_p are the roots of $\sin\eta_p l=0$.

The 3-D temperature distribution of the output window is given by Eq. (11) according to the inferential method from Eqs. (5)–(10):

$$T(r,z,t)=\frac{4P_0(1-\tau)}{\mathrm{k}r_0^2 l\pi\omega_0}\left\{\begin{array}{l}\left\{\sum_{m=1}^{\infty}\sum_{p=1}^{\infty}\frac{\alpha J_1(\beta_m\omega_0)[1-\exp(-\alpha l)(-1)^p]}{\beta_m J_0^2(\beta_m r_0)(\alpha^2+\eta_p^2)(\beta_m^2+\eta_p^2)}J_0(\beta_m r)\cos(\eta_p z)\times\left\{1-\exp\left[-\frac{k}{\rho C}(\beta_m^2+\eta_p^2)t\right]\right\}\right\}\\ +\left\{\sum_{m=1}^{\infty}\frac{J_1(\beta_m r)[1-\exp(-\alpha l)]}{2\alpha J_0^2(\beta_m r_0)\beta_m^4}J_0(\beta_m r)\left[1-\exp\left(-\frac{k}{\rho C}\beta_m^2 t\right)\right]\right\}\\ +\left\{\sum_{m=1}^{\infty}\frac{\alpha\omega_0 J_1(\beta_m r)[1-\exp(-\alpha l)(-1)^p]}{2\eta_p^2(\alpha^2+\eta_p^2)}\cos(\eta_p z)\left[1-\exp\left(-\frac{k}{\rho C}\beta_m^2 t\right)\right]\right\}\end{array}\right\}$$
$$+\frac{P_0(1-\tau)[1-\exp(-\alpha l)]}{\pi\alpha\rho C r_0^2 l}t+T_\infty. \tag{11}$$

The nonuniform temperature distribution experienced by the output window causes mechanical stresses, which can be obtained from the stress-strain equation and Hooke equation[20]

$$\sigma_r=\frac{\eta E}{1-\nu}\left(\frac{1}{r_0^2}\int_0^{r_0}Tr\mathrm{d}r-\frac{1}{r^2}\int_0^{r}Tr\mathrm{d}r\right), \tag{12}$$

$$\sigma_\varphi=\frac{\eta E}{1-\nu}\left(\frac{1}{r_0^2}\int_0^{r_0}Tr\mathrm{d}r+\frac{1}{r^2}\int_0^{r}Tr\mathrm{d}r-T\right), \tag{13}$$

$$\sigma_z=\frac{\eta E}{1-\nu}\left(\frac{2}{r_0^2}\int_0^{r_0}Tr\mathrm{d}r-T\right), \tag{14}$$

where σ_r, σ_φ, and σ_z are the thermal stresses in the radius, hoop, and axial directions, respectively; η is the thermal coefficient of expansion; E is the Young's modulus; and υ is the Poisson's ratio. Introducing the temperature distribution of Eq. (11) into Eqs. (12)–(14), we get the stress distributions of the output window

$$\sigma_r=-\frac{4\eta E P_0(1-\tau)}{\mathrm{k}r_0^2 l\pi\omega_0(1-\nu)}\left\{\begin{array}{l}\left\{\sum_{m=1}^{\infty}\sum_{p=1}^{\infty}\frac{\alpha J_1(\beta_m\omega_0)[1-\exp(-\alpha l)(-1)^p]}{\beta_m^2 J_0^2(\beta_m r_0)(\alpha^2+\eta_p^2)(\beta_m^2+\eta_p^2)}\frac{J_1(\beta_m r)}{r}\cos(\eta_p z)\times\left\{1-\exp\left[-\frac{k}{\rho C}(\beta_m^2+\eta_p^2)t\right]\right\}\right\}\\ +\sum_{m=1}^{\infty}\frac{J_1(\beta_m r)[1-\exp(-\alpha l)]}{2\alpha J_0^2(\beta_m r_0)\beta_m^4}\frac{J_1(\beta_m r)}{r}\left[1-\exp\left(-\frac{k}{\rho C}\beta_m^2 t\right)\right]\end{array}\right\} \tag{15}$$

$$\sigma_\varphi=\frac{4\eta E P_0(1-\tau)}{\mathrm{k}r_0^2 l\pi\omega_0(1-\nu)}\left\{\begin{array}{l}\left\{\sum_{m=1}^{\infty}\sum_{p=1}^{\infty}\frac{\alpha J_1(\beta_m\omega_0)[1-\exp(-\alpha l)(-1)^p]}{\beta_m J_0^2(\beta_m r_0)(\alpha^2+\eta_p^2)(\beta_m^2+\eta_p^2)}\left[\frac{J_1(\beta_m r)}{\beta_m r}-J_0(\beta_m r)\right]\frac{J_1(\beta_m r)}{r}\cos(\eta_p z)\times\left\{1-\exp\left[-\frac{k}{\rho C}(\beta_m^2+\eta_p^2)t\right]\right\}\right\}\\ +\sum_{m=1}^{\infty}\frac{J_1(\beta_m r)[1-\exp(-\alpha l)]}{2\alpha J_0^2(\beta_m r_0)\beta_m^3}\left[\frac{J_1(\beta_m r)}{\beta_m r}-J_0(\beta_m r)\right]\left[1-\exp\left(-\frac{k}{\rho C}\beta_m^2 t\right)\right]\end{array}\right\} \tag{16}$$

$$\sigma_z=-\frac{4\eta E P_0(1-\tau)}{\mathrm{k}r_0^2 l\pi\omega_0(1-\nu)}\left\{\begin{array}{l}\left\{\sum_{m=1}^{\infty}\sum_{p=1}^{\infty}\frac{\alpha J_1(\beta_m\omega_0)[1-\exp(-\alpha l)(-1)^p]}{\beta_m^2 J_0^2(\beta_m r_0)(\alpha^2+\eta_p^2)(\beta_m^2+\eta_p^2)}J_0(\beta_m r)\cos(\eta_p z)\times\left\{1-\exp\left[-\frac{k}{\rho C}(\beta_m^2+\eta_p^2)t\right]\right\}\right\}\\ +\sum_{m=1}^{\infty}\frac{J_1(\beta_m r)[1-\exp(-\alpha l)]}{2\alpha J_0^2(\beta_m r_0)\beta_m^4}J_0(\beta_m r)\left[1-\exp\left(-\frac{k}{\rho C}\beta_m^2 t\right)\right]\end{array}\right\}. \tag{17}$$

4 Numerical Computation and Discussions

In this section, some numerical calculations concerning the thermal–mechanical effects are performed, and the damage mechanism of the laser output window is investigated in the case of taking infrared quartz glass as the output window. Infrared quartz glass is used as the 2-μm laser optical window material owing to its fine performance, whose application wavelength is in the range of 260 to 3500 μm and the infrared transmittance τ is 85%. Some parameters of the glass in the calculation are listed in Table 1. We assume that the diameter D and the thickness L of the window are, respectively, 25 and 6 mm, the laser beam radius ω_0 is 2 mm, and the ambient temperature T_∞ is 20°C.

4.1 *Analysis of Temperature and Stress Fields*

Figure 3 illustrates the 3-D temperature distribution of the window in the case of a laser system producing continuous output for 8 s when the laser output power density is 1 kW/cm^2. Figure 4 displays the temperature distributions of the window surface ($L=0$) for different laser-beam radii and different durations when the laser operates at a maximum output power of 115 W.

As can be seen in Fig. 3, in the radius direction, the nearer the sample is to the center of the window, the higher the temperature is, whereas in the axial direction, the temperature does not change significantly. At the edge of the laser beam, the temperature gradient increases sharply, reflecting the thermal expansion of the actively heated area against the passively heated area of the window. Figure 4 shows that the temperature rises higher with longer run times and larger laser-beam radii. It can also be seen that the maximum temperature rise is 289°C when the laser operates at maximum output power.

Figures 5(a), 5(b), and 5(c) depict the stress distributions of the window in the radial, hoop, and axial directions,

Table 1 Physical parameters of infrared quartz glass.

Density, ρ (g/cm^3)	2.2
Heat capacity, C (J/g °C)	0.67
Thermal conductivity, k (W/cm °C)	0.014
Absorption coefficient, α_v (cm^{-1})	1×10^{-4}
Poisson's ratio, v	0.16
Young's modulus, E (MPa)	72,000
Thermal coefficient of expansion η (°C^{-1})	5.5×10^{-7}

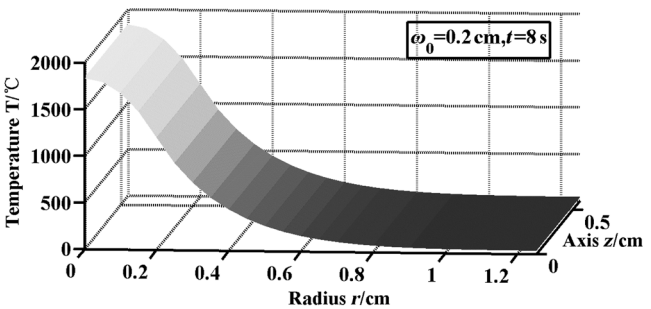

Fig. 3 Temperature distribution of the output window for a continuous wave (cw) beam of radius 2 mm with a duration of 8 s.

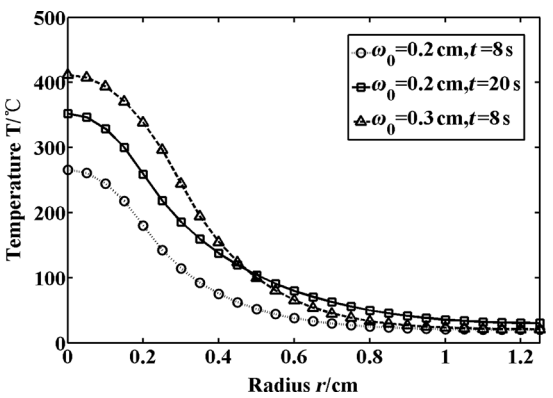

Fig. 4 Temperature distribution over the output window for different beam sizes and irradiance times.

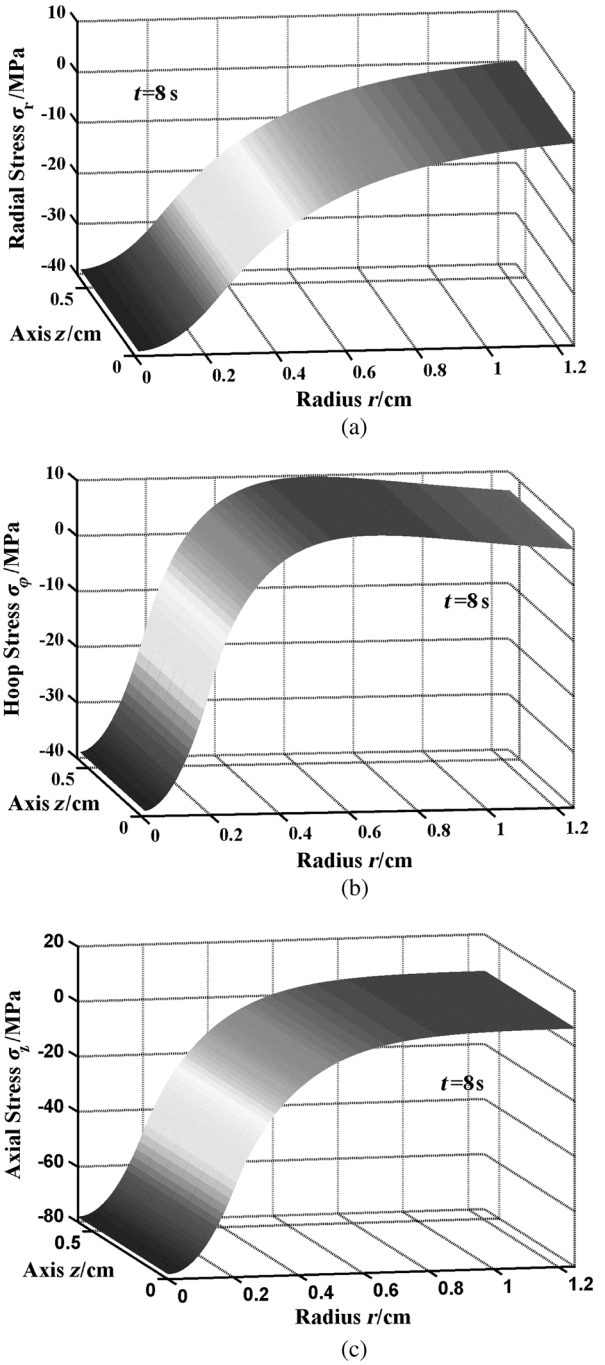

Fig. 5 Spatial dependence of the stress on the output window in the (a) radial, (b) hoop, and (c) axial directions.

respectively. Figures 6(a), 6(b), and 6(c) illustrate the situation for different run times and different laser-beam radii, all of which depict how the radial, hoop, and axial stresses evolve at the window surface ($L = 0$) when the laser operates at the maximum output power.

From Fig. 5, it can be seen that all stresses are compressive on the centerline of the window, where the maximum heat deposition occurs. Radial stress is always compressive; the hoop and axial stresses, however, turn tensile at the outer rim of the window. Figure 6 illustrates that the stress gradients become greater with longer run times or larger laser-beam radii.

4.2 *Damage Mechanism Analysis*

The infrared quartz window may be damaged because of either the temperature reaching the melting point (1780°C) or the tensile (compressive) stress exceeding the tensile (compressive) strength of 48 MPa (1100 MPa). From the analysis mentioned above, it can be seen that the temperature of window would exceed the melting point while the thermal stresses would not reach the limits, providing that the laser power density reaches 1 kW/cm^2 and the continuous laser output lasts for 8 s. The thermal stress on the quartz material caused by the temperature gradient are relatively small due to the good thermal stability of the quartz; thus the window is

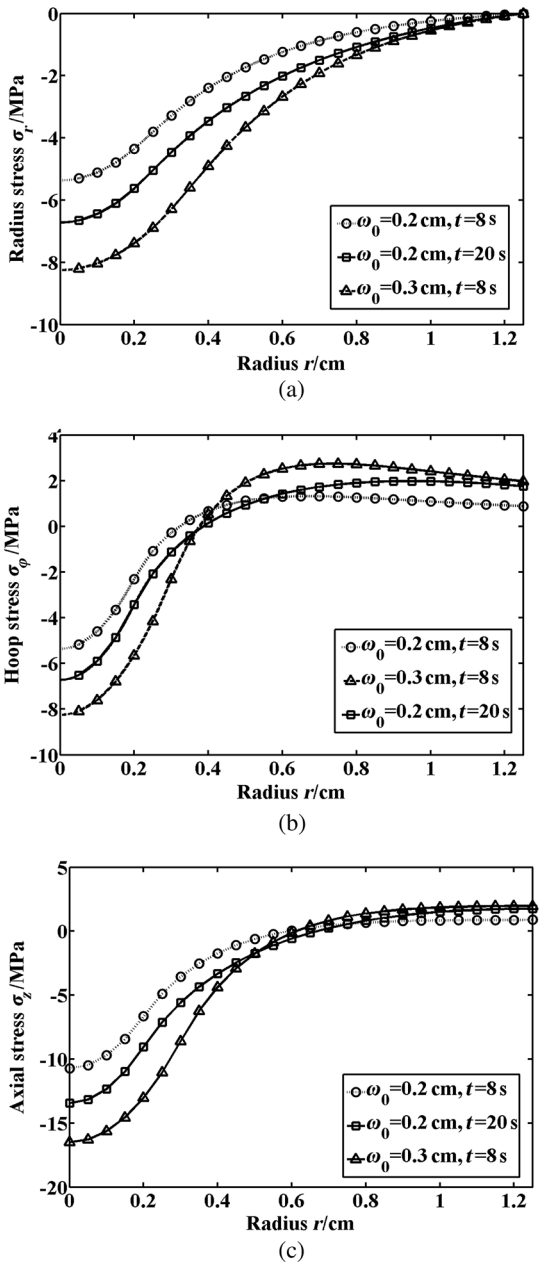

Fig. 6 Stress distributions on the output window in the (a) radial, (b) hoop, and (c) axial directions for different values of beam sizes and exposure times.

primarily damaged by melting in the area where the temperature exceeds the melting point of the material, so that melting, ablation, or even perforation arises as a result.

5 Laser Output

The wavelength of the 2-μm laser system can switch depending on the transmission of the output window. When the coupler M2 has a transmission of 10%, the wavelength of the output laser is 2.02 μm, and the maximum cw output power is 77.1 W. When the coupler has a transmission of 5%, the wavelength of the laser output is shifted to 2.07 μm, and the maximum cw output power is 115 W. The laser spectra at the maximum output power were recorded by an optical spectrometer (NIRQuest256-2.5), as shown in Fig. 7.

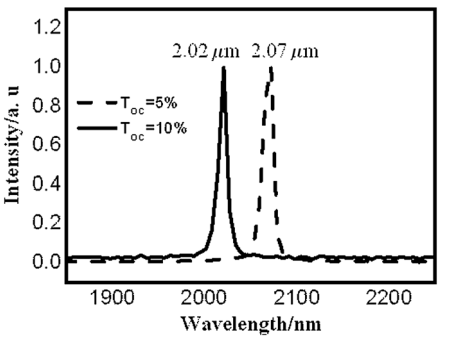

Fig. 7 Laser output spectra at the maximum output power for output couplers with transmissions of 5% and 10%.

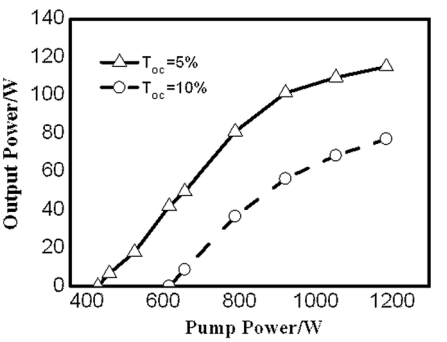

Fig. 8 Dependence of the laser output power on the pump power.

Damage to the output window can be avoided by controlling the output power of the laser system. The dependence of the laser output power on the LD pump power is obtained with a power meter (Ophir F300A-SH), as illustrated in Fig. 8. With a coupler transmission of 5%, the maximum output power is 115 W under an LD pump power of 1188 W, while the maximum power of 77.1 W is achieved with a coupler transmission of 10% under an LD pump power of 1188 W.

6 Conclusions

In summary, we have defined a thermal model of a laser window and deduced expressions for the transient thermal and mechanical distributions. Taking the infrared quartz glass as an example, the temperature and mechanical field distributions of a high-power all-solid-state 2-μm laser system window were simulated, and the laser-induced damage mechanism was analyzed. The results showed that the window damage mechanism is mainly due to the melting in the areas where the temperature exceeds the melting point of the material, when a 2-μm high-power laser continuously outputs the optical power. We believe that the research methods and results presented in this article will be helpful for the selection of laser windows.

Acknowledgments

This work was supported by the National Natural Science Foundation under Grant No. 61074158 (China).

References

1. Q. L. Ma et al., "Light scattering and 2 μm laser performance of Tm: YAG ceramic," *Opt. Commun.* **284**(6), 1645–1674 (2011).

2. B. Q. Yao et al., "Continuous-wave operation of a room-temperature Tm:YAG-pumped Ho:YAG laser," *Chin. Opt. Lett.* **6**(7), 520–522 (2008).
3. J. Yu et al., "1 J/pulse Q-switched 2 μm solid-state laser," *Opt. Lett.* **31**(4), 462–464 (2006).
4. L. Wang et al., "Resonantly pumped monolithic nonplanar Ho:YAG ring laser with high-power single-frequency laser output at 2122 nm," *Opt. Express* **21**(8), 9541–9546 (2013).
5. H. J. Liu et al., "Experimental comparison of damage performance induced by nanosecond 1ω laser between K9 and fused silica optics," *Acta Phys. Sin.* **61**(7), 076103 (2012).
6. M. E. Innocenzi et al., "Thermal modeling of continuous-wave end-pumped solid-state lasers," *Appl. Phys. Lett.* **56**(19), 1831–1833 (1990).
7. Y. X. Pan et al., "Effect of inclusion matrix model on temperature and thermal stress fields of K9-glass damaged by long-pulse laser," *Opt. Eng.* **52**(4), 044302 (2013).
8. A. S. Epifanov, A. A. Manenkov, and A. M. Prokhorov, "Theory of avalanche ionization induced in transparent dielectrics by an electromagnetic field," *Sov. Phys. JETP* **43**(2), 377–381 (1976).
9. C. L. Wang et al., "Wavelength switchable high-power diode-side-pumped rod Tm: YAG laser around 2 μm," *Opt. Express* **21**(6), 7156–7161 (2013).
10. F. Huang, Y. X. Niu, and Y.F. Wang, "Calculation of thermal and mechanical effect induced by laser in optical window materials," *Acta Opt. Sin.* **26**(4), 576–580 (2006).
11. C. A. Klein, "High-energy laser windows: case of fused silica," *Opt. Eng.* **49**(9), 091006 (2010).
12. Y. F. Peng et al., "Laser-induced temperature distributions and thermal deformations in sapphire, silicon, and calcium fluoride substrates at 1.315 μm," *Opt. Eng.* **40**(12), 2822–2829 (2001).
13. Y. X. Niu et al., "Thermal shock effect on diamond-like carbon thin films induced by pulsed-laser," *Acta Phys. Sin.* **54**(10), 4816–4821 (2005).
14. X. F. Duan, Y. X. Niu, and C. Zhang, "Calculation of laser irradiation effect and analysis of laser-induced damage threshold in semiconductor," *Acta Opt. Sin.* **24**(8), 1057–1061 (2004).
15. P. H. Lu and R. W. Wang, "Three-dimensional temperature distribution analysis and thermal lens effect calculation for high power laser windows," *Acta Opt. Sin.* **21**(8), 965–969 (2001).
16. Y. S. Feng and X. X. Li, "ANSYS numerical simulation of temperature field in silica glass irradiated by pulsed laser," *Phys. Exp.* **32**(2), 35–37 (2012).
17. J. Li et al., "Numerical analysis of CW laser damage in GaAs," *Acta Photon. Sin.* **41**(5), 571–574 (2012).
18. J. Wu et al., "Thermal effect in pulsed laser diode dual-end pumped Tm:YAG laser," *Proc. SPIE* **8904**, 890413 (2013).
19. M. N. Ozisik, *Heat Conduction*, High Education Press, Beijing (1983).
20. P. Xiuer, *Thermal Stress and Thermal Fatigue*, pp. 12–30, National Defense Industry Press, Beijing (1984).

Wenwen Liu received her BS degree in optical engineering from Beihang University, Beijing, China, in 2010. She is currently pursuing her MS degree in optical engineering at Beihang University. Her research is focused on laser technology.

Yanxiong Niu is a professor at Beihang University. His research interests include laser physics and technology and new photoelectric system design.

Biographies of the other authors are not available.